Changes of anthropogenic CO_2 and CFCs in the North Atlantic between 1981 and 2004

Toste Tanhua,[1] Arne Biastoch,[2] Arne Körtzinger,[1] Heike Lüger,[1,3] Claus Böning,[2] and Douglas W. R. Wallace[1]

Received 16 January 2006; revised 14 July 2006; accepted 10 August 2006; published 15 December 2006.

[1] We compare total dissolved inorganic carbon (DIC) and chlorofluorocarbon (CFC) measurements in the northwest Atlantic made during the Transient Tracers in the Ocean, North Atlantic Study (TTO-NAS) in 1981 with modern measurements from a cruise in 2004. The observed changes in the DIC and CFC fields are compared to those predicted from an eddy-permitting ocean circulation model. The rapid, but time-variable, atmospheric CFC increase in relation to the relatively steady anthropogenic CO_2 increase influences the relationship between the observed uptake of DIC and CFC. We demonstrate the importance of ocean mixing in the calculation of anthropogenic CO_2 (C_{ant}) based on transient tracer data by comparing our observations to a ''no-mixing'' scenario. We further find that the C_{ant} is in transient steady state in the North Atlantic; that is, the C_{ant} concentration increases proportionally over time through the whole water column in a manner that is directly related to the time-dependent surface concentration.

Citation: Tanhua, T., A. Biastoch, A. Körtzinger, H. Lüger, C. Böning, and D. W. R. Wallace (2006), Changes of anthropogenic CO_2 and CFCs in the North Atlantic between 1981 and 2004, *Global Biogeochem. Cycles*, *20*, GB4017, doi:10.1029/2006GB002695.

1. Introduction

[2] The ocean is a significant global sink for anthropogenic CO_2 (C_{ant}), and contains ~48% of the C_{ant} released to the atmosphere over the past 250 years [*Sabine et al.*, 2004]. The North Atlantic Ocean is of especially large importance and stores ~23% of the total C_{ant} despite representing only 15% of the ocean surface area. This is mainly due to the formation of deep and intermediate water masses that are advected into the ocean interior after being in contact with the atmosphere, where the ocean gets exposed to ever increasing CO_2 concentrations. High-quality inorganic carbon measurements made, for instance, during the WOCE-JGOFS Global CO_2 Survey [*Wallace*, 2001] have allowed quantification of the total inventory of anthropogenic CO_2 in North Atlantic [cf. *Gruber*, 1998; *Lee et al.*, 2003] and for the global oceans [*Sabine et al.*, 2004]. These inventory calculations refer to the cumulative uptake since ~1780 and the methods used to identify C_{ant} make a number of major assumptions. In particular, different assumptions and methods can lead to large differences in C_{ant} estimates in key regions such as the Southern Ocean [*Lo Monaco et al.*, 2005].

[3] As the database of high-quality data grows, it is possible to directly evaluate decadal changes in carbon inventories by comparing new data sets with historical ones [cf. *Wallace*, 1995; *Friis et al.*, 2005]. Such comparisons are potentially less dependent on assumptions and therefore useful for global carbon sink assessments [*Peng et al.*, 1998]. This approach is dependent on access to data sets of known and high accuracy that are separated in time by at least 1–2 decades in order that the anthropogenic increase is detectable over measurement noise and short-term variability. Possible problems with this approach include seasonal and long-term variability in the natural carbon cycle and hydrography which might mask or alias the anthropogenic transient.

[4] The GEOSECS global survey in the 1970's was the first systematic attempt to globally map the inorganic CO_2 in the oceans. One comparison to the GEOSECS data set was made using measurements made in the Indian Ocean during 1995 [*Peng et al.*, 1998], and the anthropogenic increase of the DIC inventory was quantified. The GEOSECS data set, however, suffered from technical difficulties such as titrimetric data not agreeing with pCO_2 data, and a systematic difference to modern data on the same order of magnitude as the measured DIC increase. Other studies have since then quantified the temporal changes in DIC from repeat measurements, for instance in the southern Ocean [*McNeil et al.*, 2001; *Matear and McNeil*, 2003] and the Indian Ocean [*Sabine et al.*, 1999]. Since GEOSECS, data sets of improved quality have been collected in the Atlantic during TTO, 1981–1982 [*Brewer et al.*, 1986] and SAVE, 1988–1989 (CDIAC: http://cdiac.esd.ornl.gov/ftp/

[1]Marine Biogeochemie, Leibniz-Institut für Meereswissenschaften an der Universität Kiel, Kiel, Germany.
[2]Ozeanzirkulation und Klimadynamik, Leibniz-Institut für Meereswissenschaften an der Universität Kiel, Kiel, Germany.
[3]Now at Cooperative Institute of Marine and Atmospheric Science, Miami, Florida, USA.

0886-6236/06/2006GB002695

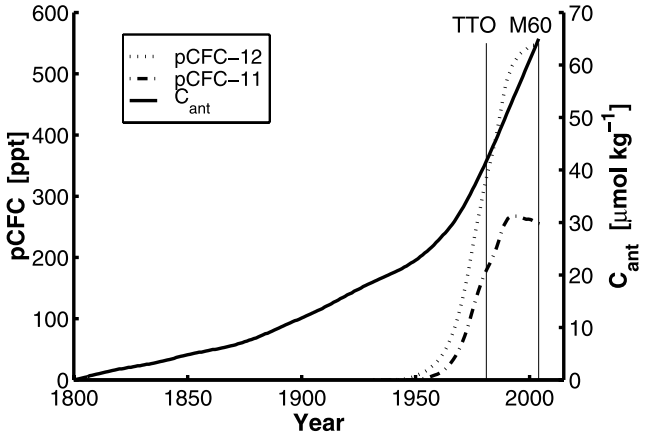

Figure 1. Expected surface water concentrations of pCFC-12, pCFC-11 and anthropogenic DIC in the North Atlantic subtropical gyre (Revelle Factor 9.7). The CFCs and DIC are assumed to be in equilibrium with the atmosphere. Anthropogenic DIC is calculated using the CO2SYS program [*Lewis and Wallace*, 1998] with the transient anthropogenic CO_2 atmospheric concentration as described in section 3, together with typical and constant values of alkalinity, phosphate and silicate. The CFC-11 and -12 input functions are from *Walker et al.* [2000], extended with yearly mean values from Northern Hemisphere AGAGE sampling stations, available from http://cdiac.esd.ornl.gov/ftp/ale_gage_Agage/.

oceans/save/) and globally during WOCE, 1990–1998 [*Wallace*, 2001]. This implies that with repeat measurements of historical cruises, this approach can now be applied globally.

[5] The earliest basin-wide data set suitable for direct evaluation of C_{ant} in the North Atlantic was collected during the Transient Tracers in the Ocean North Atlantic Study (TTO-NAS) in 1981. During the TTO-NAS experiment, high-quality measurements of alkalinity and DIC were made with considerably better accuracy and precision than was achieved for the GEOSECS data set. A systematic evaluation of the accuracy, precision and consistency of the TTO-NAS DIC and alkalinity data relative to modern data standards has been reported recently [*Tanhua and Wallace*, 2005]. On the basis of this analysis the TTO-NAS DIC measurements provide a solid base for examining and documenting the chemical changes taking place in the North Atlantic Ocean.

[6] Information concerning oceanic ventilation and oceanic transport times is of importance for estimating and understanding the oceanic sink of anthropogenic CO_2. Measurements of anthropogenic transient tracers such as CFCs provide useful information on these quantities by direct measurement [e.g., *Schlosser et al.*, 2001]. Not only the tracer field, but also the change in the CFC transient tracer field determined from repeat hydrographic sampling can be used to estimate the ventilation of the ocean as shown by *Doney et al.* [1997]. The transient atmospheric CFC and C_{ant} signals are the key to these estimates, and they are portrayed in Figure 1. By making the oversimplistic assumption of the absence of mixing (i.e., assuming purely advective transport of CFC and DIC) and assuming an invariant ocean circulation, the expected change in concentration is plotted as a function of apparent age of water masses in Figure 2.

[7] In order to explore the information contained in the earliest quality measurements of DIC and CFC in the North Atlantic, we designed a cruise in 2004 which sought to reoccupy as many TTO-NAS stations as possible. The aim of this study is to review the changes of both DIC and CFC-11 in the North Atlantic as determined from direct measurements performed at 10 stations that have been sampled for both parameters, 23 years apart, focusing on changes that occurs below the thermocline. We then compare the observations with the results from a eddy-permitting ocean circulation model (FLAME) that includes CFC-11 and C_{ant}. In this way we determine to what extent we can use the model to learn about the real ocean, and then let the model guide us in the interpretation of the observations.

2. Methods

[8] The cruise 60, leg 5 (M60/5) of the German research vessel *Meteor* left the port of Fort-de-France (Martinique) on 10 March 2004 and arrived in Lisbon, Portugal on 13 April 2004. The cruise tracks of the two campaigns (Figure 3) enabled resampling of 10 stations where both

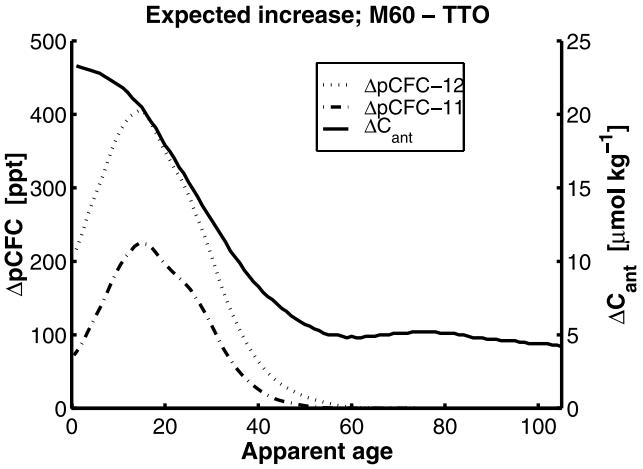

Figure 2. Expected increase in seawater concentrations between 1981 and 2004 for pCFC-12, pCFC-11 and DIC in a water sample, measured in 2004, as a function of apparent age. We have neglected the effects of mixing, i.e., we assume purely advective transport, so that the time-dependent surface concentration of the CFCs and DIC is maintained in the water parcel as it is transported from the outcrop region to the interior ocean. We also assume that any offsets to the thermodynamic equilibrium for CFC and DIC with respect to the atmosphere is constant in time, in addition to using the same data and assumptions as in Figure 1. The maximum in ΔCFC that is seen for a water parcel of "age" about 20 years is thus an upper limit before the atmospheric concentrations started to level off or decrease.

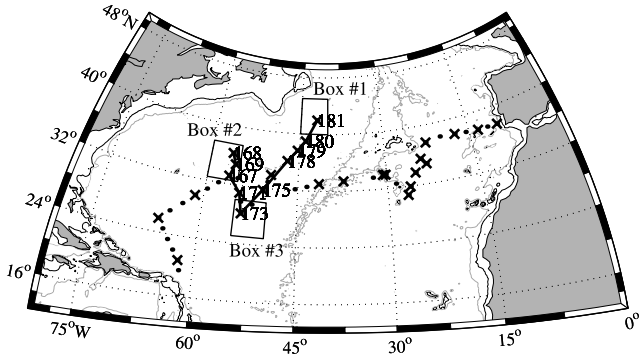

Figure 3. Map of the cruise track of the *Meteor* cruise M60/5 in 2004 (dots). Stations marked with a cross denote stations where a station was sampled also during the TTO-NAS experiment in 1981. Numbered stations denotes stations where also CFCs were measured during TTO-NAS. The two lines identify the positions of the sections, and the boxes denote domains used for the model comparisons.

DIC and CFCs were measured during TTO-NAS, leg 7 (CFCs were only measured on leg 7 of TTO-NAS).

2.1. CFC Data

[9] The CFC tracer measured during leg 7 of the TTO-NAS experiment in 1981 represent some of the very earliest quality measurements of CFC from the ocean interior [*Weiss et al.*, 1985], hence the data quality might not be as good as that of the modern (WOCE) standard, but are still regarded to be of reasonably high quality, and a good measure of the CFC field in the early 1980s. The CFC measurements were performed by R. H. Gammon, and were later recalibrated to the SIO98 calibration scale (J. L. Bullister, personal communication, 2004).

[10] The CFC measurements performed during M60/5 were made on an analytical system similar to that described by [*Bullister and Weiss*, 1988], and are also reported on the SIO98 scale. The analytical precision was determined to be 0.7 and 0.6% for CFC-12 and CFC-11, respectively, as calculated from duplicate samples, typically at two depths per station. The relative changes in CFC concentration between TTO and M60/5 are large, and a small analytical error (TTO and/or M60/5) will not affect the general pattern of north Atlantic ventilation revealed over this time frame. The combined analytical error for the CFC measurements during TTO and M60/5 is estimated to be of the order of 3%.

[11] To eliminate the effects of variable temperature and salinity on the CFC solubility, we generally report the CFC-11 concentrations, C_{CFC}, as dry air CFC mole fraction of a gas phase that is in equilibrium with the seawater sample, pCFC, where

$$pCFC = \frac{C_{CFC}}{F(\theta, S)}.$$

[12] The salinity and temperature-dependent solubility of the tracers, $F(\theta,S)$, are calculated from the solubility functions reported by *Warner and Weiss* [1985]. We have assumed that the atmospheric pressure is 1 atm over the surveyed area. The dry air mole fractions are the units in which the atmospheric histories are presented by *Walker et al.* [2000]. This presentation also allows the measured CFC-11 data to be compared directly with the reported atmospheric CFC histories.

[13] In this work we will discuss changes in the tracer pCFC-11 (i.e., the ΔpCFC-11) to facilitate comparison with modeled pCFC-11 values. The pCFC-12 data, however, also support the conclusions reported here. The atmospheric concentration of CFC-11 has increased from 183 to about 255 ppt between 1981 and 2004 (Figure 1), i.e., ΔpCFC-11(atm) = 72 ppt. However, since the atmospheric concentration of CFC-11 has decreased since the mid 1990s after an earlier period of rapid increase, the maximum in ΔpCFC-11 would be expected in water parcels formed around 1990, i.e., with an apparent age of about 14 years (relative to 2004) for which the maximum ΔpCFC-11 would be 224 ppt (Figure 2).

2.2. Inorganic Carbon Data

[14] Direct measurements of DIC and total alkalinity were made during *Meteor* 60/5 using coulometric [*Johnson et al.*, 1993] and potentiometric titration [*Mintrop et al.*, 2000] methods, respectively. In the case of DIC, the measurements were calibrated independently by regular injections of known amounts of pure CO_2 [*Department of Energy*, 1994]. The accuracy of both methods was assessed by regular measurement of Certified Reference Materials (CRM, supplied by Andrew Dickson, Scripps Institution of Oceanography (SIO), La Jolla, CA) from 4 separate batches (batch 58, 60, 63 and 64) which gave a mean offset between our measurements and the Certified Values of 1.02 ± 0.44 μmol kg^{-1} (95% confidence interval, n = 88). Measured DIC concentrations were adjusted to the certified calibration scale by subtraction of this mean offset. Precision of the measurements was 1.49 μmol kg^{-1} (95% confidence interval), as determined from analyses of duplicate samples.

[15] The TTO-NAS data were downloaded from the Carbon Dioxide Information and Analysis Centre (CDIAC;http://cdiac.esd.ornl.gov/oceans/ndp_004/ndp004.html). The reproducibility of the titrimetric alkalinity data is reported to be 3.5 μmol kg^{-1}, and for pCO_2 the reproducibility is reported to be 0.1% [*Brewer et al.*, 1986]. By carefully comparing TTO-NAS alkalinity and DIC data with the corresponding data from the deep eastern basin measured during M60/5, and with contemporaneous manometric measurements of DIC samples collected during TTO-NAS experiment made in the lab of C. D. Keeling at SIO [*Gruber et al.*, 1996], *Tanhua and Wallace* [2005] recommended small corrections to the TTO-NAS carbonate system data set in order to make the TTO-NAS inorganic carbon data set consistent with modern data. Here we have applied those corrections to the TTO-NAS data. The combined analytical error for the DIC measurements during TTO and M60/5 is estimated to 4.0 μmol kg^{-1}, whereas the corresponding number for the alkalinity measurements is 5.5 μmol kg^{-1} [*Tanhua and Wallace*, 2005].

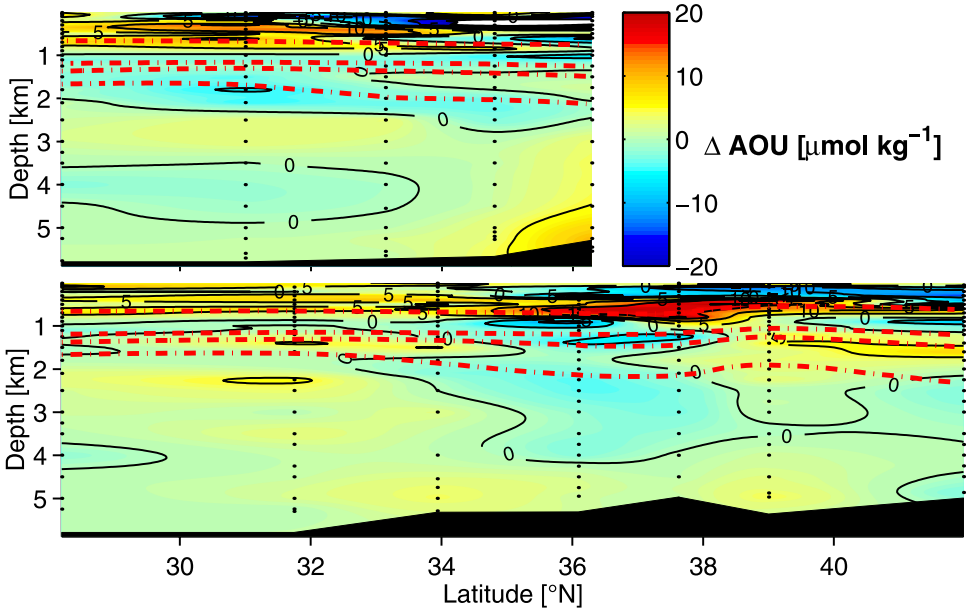

Figure 4. Sections of changes in Apparent Oxygen Utilization (ΔAOU) between 1981 and 2004 for the two sections indicated in Figure 3. The dash-dotted lines are the σ_θ surfaces 27.00, 27.68. 27.74 and 27.8, encompassing the AAIW, uLSW and LSW density layers. Bottom topography is determined solely from the depth at the stations.

[16] The ΔDIC values we present have been corrected for changes in remineralization of organic matter and dissolution of calcium carbonate using the relation;

$$DIC_{bio} = \Delta DIC - 0.746 \times \Delta AOU - 0.5 \times (\Delta Alk + \Delta NO_3)$$

where DIC_{bio} is the biology compensated DIC, and the Δ-symbol denotes a change in properties between M60 and TTO (M60/5-TTO). The factor 0.746 is the C/$-O_2$ ratio of remineralization as calculated for the Northeast Atlantic Ocean by *Körtzinger et al.* [2001], and the factor 0.5 is the effect on DIC by change in alkalinity during dissolution of calcium carbonate (ΔAlk). The proton flux during respiration and remineralization assumed to be proportional to changes in nitrate (ΔNO_3). In this way, we only correct for the differences in oxygen, alkalinity and nitrate between the TTO-NAS and M60/5 cruises. The change in oxygen concentration between the two cruises is generally less than 5–7 μmol kg^{-1} below the thermocline, although larger changes within the thermocline is observed (Figure 4). The maximum error introduced to the calculation of DIC changes, ΔDIC_{bio}, below the thermocline associated with an error in the respiratory quotient C/-O_2 is thus 7 times the error in the remineralization ratio, i.e., 0.5 μmol kg^{-1} assuming that the respiratory quotient is known to ±0.1 units. The combined analytical uncertainty in determining the DIC_{bio} is estimated to be 5.0 μmol kg^{-1} on the basis of the combination of above mentioned errors.

[17] Having done the corrections for the biological part of the changing DIC signal, we assume that the ΔDIC_{bio} is due solely to the perturbation of anthropogenic CO_2 [c.f. *Friis*, 2006]. However, temporal changes in surface alkalinity, or changes in ventilation that alter the relation between O_2 and CO_2 saturations, can cause the ΔDIC_{bio} to not only represent anthropogenic CO_2 changes (ΔC_{ant}). Differences between ΔDIC_{bio} and ΔC_{ant} are however estimated to be small in comparison to the observed ΔDIC_{bio}, which is confirmed by comparison to the model that predicts the anthropogenic CO_2 without any biological processes.

2.3. Comparison of TTO-NAS With M60/5

[18] The position of the 10 stations where we have observations of DIC for both the TTO-NAS and the M60/5 cruises are the numbered stations shown in Figure 3. For each repeat station (i.e., a TTO-NAS and a M60/5 station at the same position) the profiles have been compared on neutral density surfaces between 200 and 2000 m depth. In contrast, values close to the surface and deep samples were always compared by depth, independent of any changes in density between the repeats. A new depth vector for the TTO data was constructed to make the density profiles for the two cruises identical for the depth interval 200–2000 m. The TTO data have then been interpolated to the sample depths of the M60/5 repeat. The profile of change in any parameter is, in this way, displayed at the depths of the M60/5 sampling, independent of the actual sampling depths for the TTO repeat. The comparison of the two cruises has therefore been made both in density and depth space, but is visualized only in depth space. This means that changes in the vertical position of the pycnocline, with its sharp gradient in properties, are, at least partly, compensated for by comparison on density surfaces rather than depth. Since we are not comparing or calculating inventories, any changes in the density profiles between the cruises do not

affect the results presented here. For samples within the thermocline, however, the sharp gradient of properties is an additional source of error for the difference calculations due to difficulties to perfectly match up the profiles of the repeat sampling.

3. Model

[19] The model used here is a 3D ocean general circulation model (OGCM) with realistic bottom topography and surface forcing. The configuration is based on the "Modular Ocean Model" (MOM) [*Pacanowski*, 1996] with extensive modifications to enable the use of high-performance computers and to implement processes important for the large-scale thermohaline circulation, such as a bottom boundary layer parameterization to correctly represent the effect of the overflow across the Greenland-Scotland Ridge. This configuration is a well tested component in the "Family of Linked Atlantic Model Experiments" (FLAME) [*Böning et al.*, 2003; *Getzlaff et al.*, 2005]. The model domain covers the Atlantic Ocean with open boundaries in the Drake Passage and south of Africa, whereas at the northern boundary at 70°N and off the Strait of Gibraltar the temperature and salinity fields are relaxed toward climatological data. The resolution is $1/3° \times 1/3°$ cos(lat) with 45 z-levels; that is, the model is, except for the subpolar regions, "eddy-permitting." The remaining, small-scale part of the spectrum is parameterized by the *Gent and McWilliams* [1990] approach.

[20] The model was initialized by temperature and salinity fields from observations [*Boyer and Levitus*, 1997] and spun up for 25 years. After that the atmospheric increase of anthropogenic CO_2 and CFC-11 was initialized and the model was integrated for the first 57 years (1900–1957) using a repeated-year wind stress and heat flux formulation [*Barnier et al.*, 1995] with atmospheric data based on the ECMWF model. For the time period 1958–2001 the model was forced by interannually varying thermal forcing and wind stress data based on the NCEP reanalysis products [*Kistler et al.*, 2001]. The freshwater component was replaced by restoring sea surface salinity to monthly observations.

[21] The geochemical part of the model is based on the assumption that the natural carbon cycle was in steady state in preindustrial times and that the biological pump has not been changed by human influence; that is, the anthropogenic part of the carbon can be separated from the natural cycle and modeled as an inert tracer [*Sarmiento et al.*, 1992; *Siegenthaler and Joos*, 1992]. Variations in surface alkalinity are estimated from salinity and temperature using the relations determined by *Lee et al.* [1997]. The atmospheric anthropogenic pCO_2 is determined from a combination of measurements [*Enting et al.*, 1994] until 1990 and the IPCC scenario S650 after 1990. The C_{ant} is estimated from pCO_2 and alkalinity using the *Mehrbach et al.* [1973] dissociation constants, as refitted by *Dickson and Millero* [1987], and the gas exchange is parameterized with a quadratic wind-speed dependent piston velocity [*Wanninkhof*, 1992] using the same monthly input data as the physical model. Since the model run starts in year 1900, it neglects the first century of anthropogenic CO_2 input and hence likely underestimates the C_{ant} in the older waters.

[22] CFC-11 was modeled similarly to anthropogenic CO_2 with the appropriate input function (Figure 1), solubility and air-sea exchange coefficient. The CFC-11 atmospheric concentrations for the 45 years from 1931 to1996 (R. F. Weiss, personal communication, 1996) were extrapolated to 2001 by keeping CFC-11 constant, which will cause a small error in the most recently ventilated waters since, in reality, the CFC-11 atmospheric concentration did decrease between 1996 and 2001. The modeled 23 year change in pCFC-11 and DIC are thus for the period between 1978 and 2001, i.e., shifted by three years compared to the observations since the model only runs through 2001.

[23] The uptake and spreading of anthropogenic CO_2 and CFC-11 as calculated by the model has been studied by A. Biastoch et al. (Uptake and spreading of anthropogenic trace gases in an eddy-permitting model of the Atlantic Ocean, submitted to *Journal of Geophysical Research*, 2006), who verify the model in terms of large-scale distribution and integral quantities and further points out the close interplay of the physical circulation and tracers, reflected in a mesoscale structure of the anthropogenic CO_2 uptake in the subpolar North Atlantic and a close correlation of the variability in the meridional overturning circulation and the northward transport of anthropogenic CO_2. The model's ability to simulate CFC inventories and formation rates in the LSW has been investigated by *Böning et al.* [2003]. The model shows large temporal variations in the CFC uptake that correlate with the North Atlantic Oscillation Index (with a one year time lag), and seems to realistically simulate the major aspects of the interannual variability of convection in the Labrador Sea.

4. Observations of Changes in DIC and pCFC-11

[24] We start the discussion of the change in the pCFC-11 and DIC concentrations, calculated as described in section 2.3, by presenting the repeat sections interpolated using objective mapping. The topography is determined by the depth at the stations. The ΔpCFC-11 and ΔDIC values predicted from the annual averages of the model are presented as sections that closely follow the actual positions of the observations. The model results are then interpolated using objective mapping in the same way as for the observations. The modeled sections are, however, not on the exact positions of the observations, which explains the small differences in bottom topography. We then compare ΔpCFC-11 with ΔDIC, again using both observations and the model output.

[25] We first explore the pathways for the Labrador Sea Water, LSW, in Figure 5 that shows the horizontal distributions of the modeled ΔDIC and ΔpCFC-11 (2001–1978) averaged over the depth interval 1500–2500 m (the LSW layer) as well as the position of the M60 sections. The spreading of LSW from its formation region in the Labrador Sea is clearly seen as a tongue of recently ventilated water, i.e., with high ΔpCFC-11 with ΔDIC values, that reaches southwestward along the mid-Atlantic ridge to about 35°N,

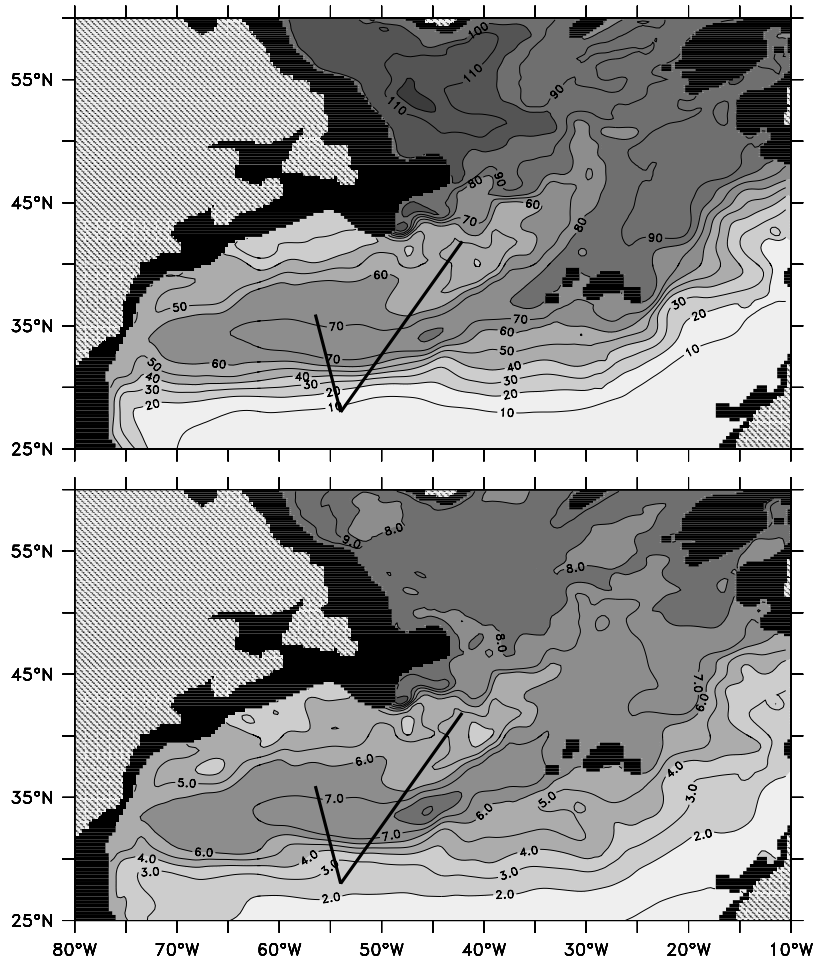

Figure 5. Modeled horizontal distribution of (top) ΔDIC and (bottom) ΔpCFC-11 between 1978 and 2001. The data are averaged over 1500–2500 m to produce a representative picture of the LSW distribution. The black lines are the location of the observed sections. Land is marked with a black and white raster and areas shallower than 1500 m are marked in black.

where the tongue leaves the ridge and flows westward across the subtropical gyre.

4.1. ΔpCFC-11

[26] The measured ΔpCFC-11 is presented in Figure 6 for the two sections (see map in Figure 3). Also indicated are the density surfaces that indicate the upward extent of (from above) Antarctic Intermediate Water (AAIW), upper Labrador Sea Water (uLSW) and Labrador Sea Water (LSW). The ΔpCFC-11 in the surface layer reflects the increase in atmospheric CFC-11 concentration of about 72 ppt. The subsurface ΔpCFC-11 maximum, seen in both sections in the thermocline at about 500–700 meters, is a sign of waters with an apparent age of about 15 years, at the end of the period of rapid CFC atmospheric increase (Figure 2). This maximum has however been eroded by mixing with surrounding water masses and the maximum change is therefore about only 120 ppt, to be compared with the maximum ΔCFC-11 value of about 220 ppt for the, hypothetical, case with no mixing in the ocean (Figure 2). There is no corresponding maximum evident in a section of the absolute pCFC-11 values measured during the M60/5 cruise (Figure 7), illustrating the effect of the different source functions of pCFC-11 and ΔpCFC-11. A layer characterized by low oxygen and high silicate concentrations is found below this subsurface maximum of ΔpCFC-11 in the permanent thermocline in both sections, and is influenced by Antarctic Intermediate Water (AAIW). This layer shows a minimum in both ΔpCFC-11 and pCFC-11 values.

[27] The layer below the AAIW is dominated by Labrador Sea Water, LSW and uLSW which is characterized by significant values of ΔpCFC-11 of >80 ppt and pCFC-11 > 120 ppt, but with large lateral variability. Along these sections we cannot detect any significant and consistent differences between the uLSW and LSW layers. The uLSW density layer is confined to a thin layer within the sections, indicating that formation of LSW dominated over that of uLSW at the time of formation. We thus find evidence for the modeled distribution of LSW (Figure 5) in the two sections from M60/5, although the modeled tongue appears about 2° of latitude further south com-

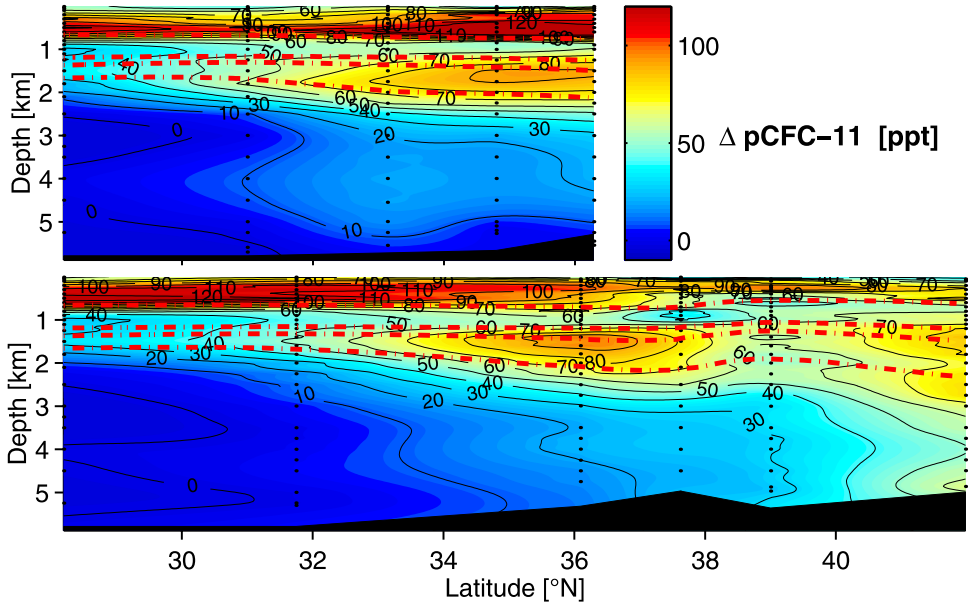

Figure 6. Sections of the measured ΔpCFC-11 between 1981 and 2004 for the two sections indicated in Figure 3.

pared to our observations. This spreading pattern of LSW is not reported in recent studies of LSW pathways and CFC inventories [c.f. *Rhein et al.*, 2002; *Kieke et al.*, 2006] since these studies were conducted further north. The southward transport of LSW west of the Mid Atlantic Ridge is however evident from their data.

[28] The deep waters of the sections show a clear north-south gradient, with ΔpCFC-11values in the north of 10–20 ppt in the western section and up to 60 ppt in the eastern section, indicating advection of recently ventilated overflow waters in the north as well as volumes of water that are virtually unaffected by CFC-11 in the south.

[29] The modeled ΔpCFC-11 for the same two sections is displayed in Figure 8. These sections are on positions that make them directly comparable with the sections of observed ΔpCFC-11 in Figure 6. There are many notable similarities between the modeled and observed sections, for instance the core with about 70–90 ppt CFC-11 increase between 1000 and 2000 meters depth in a layer dominated by Labrador Sea Water. The values of ΔpCFC-11 in the well ventilated LSW

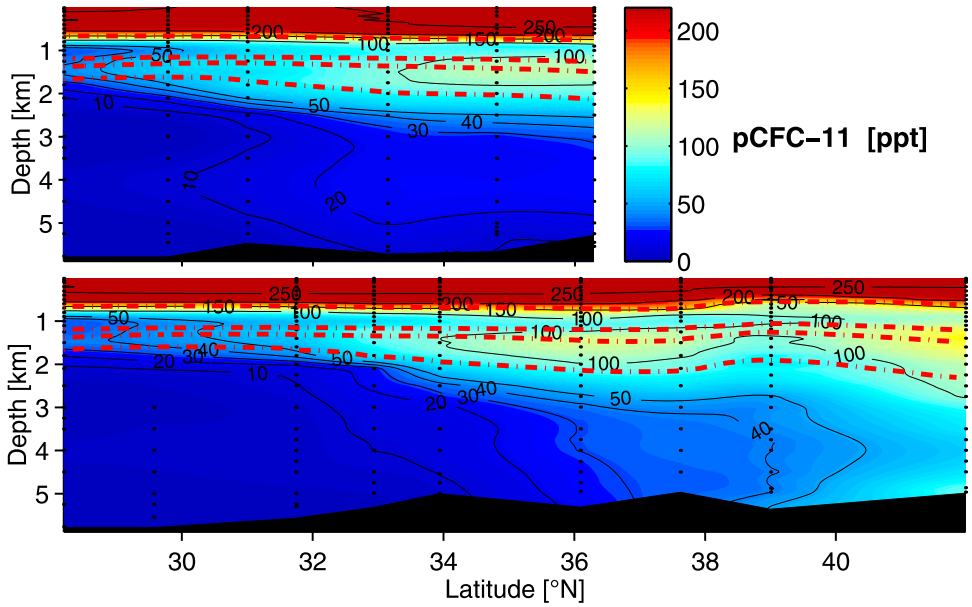

Figure 7. Sections of measured pCFC-11 during the M60/5 cruise in 2005.

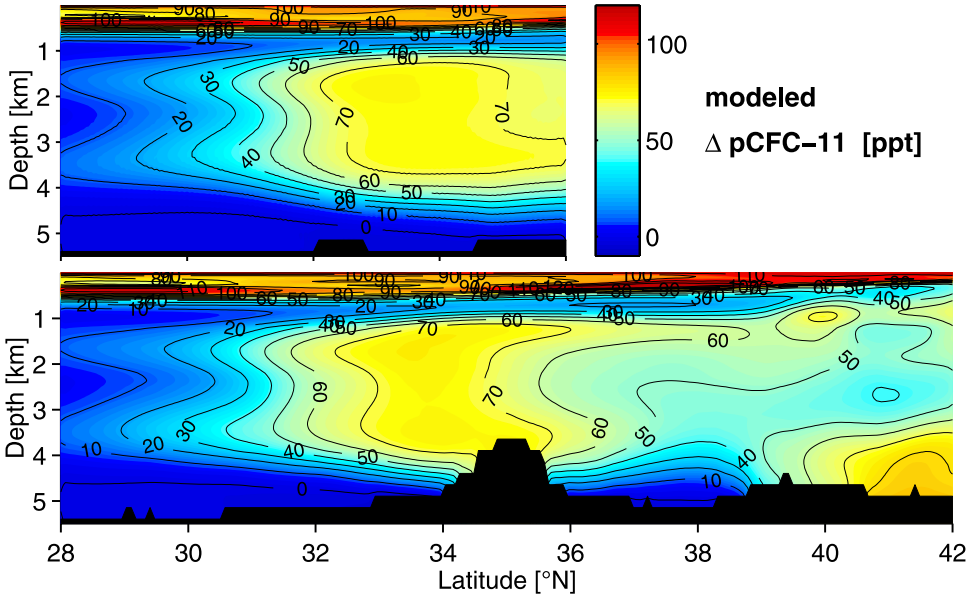

Figure 8. Sections of the annual average of modeled ΔpCFC-11 between 1978 and 2001 for the two sections indicated in Figure 3. The position of the modeled sections are close to the observed sections, but not identical, which explains the differences in topography.

layer are only slightly lower in the model compared to observations; that is, the change is modeled to be on average ~70 ppt compared to an observed value of ~80 ppt. Further the subsurface maximum of about 120 ppt in the thermocline is well represented in the model, as is the thickness of the AAIW layer with ΔpCFC-11 values <60 ppt. There are, however, also some discrepancies between the model and the observations. Most obvious is the much too deep penetration of the well ventilated LSW, which is a known deficit of this model [*Böning et al.*, 2003] that is further confirmed with this comparison to data. The LSW core is furthermore located about 2° too far south in the model compared to observations. In the AAIW layer, the ΔpCFC-11 is lower in the model compared to observations; this may suggest stronger mixing in the real ocean compared with the model, or alternatively a too long transport time for the AAIW in the model.

4.2. ΔDIC

[30] The sections of observed ΔDIC_{bio} are presented in Figure 9 (Station 177 is included in the eastern section even though there are no CFC values from TTO-NAS for this station). The increase in the upper water column is close to the expected value of 23 μmol kg^{-1} for the 23 year period (Figure 2). However, in the surface samples, especially in the northern part of the sections, larger differences were observed. This is likely due to seasonal effects since the northern part of M60/5 was sampled during late winter when nutrients were still present in the surface and the spring bloom was underway (M. Mills, personal communication, 2004), whereas TTO was sampled in late summer/early fall. Wintertime DIC values are expected to be higher owing to increased solubility (low temperature), the effect of deep mixing and low biological activity. Below the surface layer, ΔDIC_{bio} values range from 0 to 15 μmol kg^{-1}. Some of the smaller-scale variability may be due to oceanic mesoscale variability and/or measurement errors (see section 2.2), nevertheless, some key features can be seen in the sections.

[31] In contrast to the CFCs, there is no clear ΔDIC_{bio} minimum within the AAIW layer, and in the eastern section there is no significant ΔDIC_{bio} values in the LSW layer centered around 34°N where high ΔpCFC-11 is observed. Similarly to the ΔpCFC-11, in the northern part of the eastern section there are high ΔDIC_{bio} values from the thermocline to the bottom.

[32] The modeled ΔDIC is presented in Figure 10, with these sections again being directly comparable with the sections of observed ΔDIC_{bio} (Figure 9). The model results are not quite as consistent with the observed ΔDIC_{bio} as was the case for the ΔpCFC-11. With the exception of the too thick LSW layer and lack of seasonal effects in the surface, the comparison of the data and model is reasonable for the western section where the differences are generally <5 umol kg^{-1}. For the eastern section however there are clear differences between the model and the observations, particularly in the LSW layer were the modeled southward penetration of ΔDIC isolines 5–10 umol kg^{-1} is not observed.

5. Discussion

[33] In this section we describe the relationship between the observed ΔpCFC-11 and ΔDIC_{bio} and discuss the implications of the observations.

5.1. Different Input Functions

[34] The two northernmost stations (stations 180 and 181, at 39 and 42°N respectively) are in a region where the

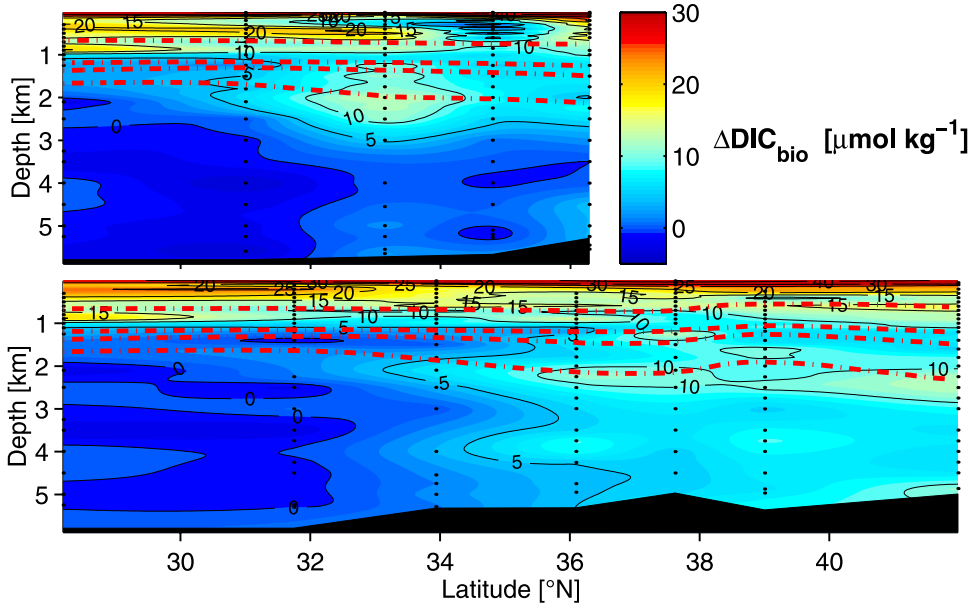

Figure 9. Sections of the measured ΔDIC_{bio} between 1981 and 2004 for the two sections indicated in Figure 3.

anthropogenic DIC and CFC signals reach through the entire water column, whereas at the southernmost station (station 173 at 28°N) there is only a minor CFC and DIC change below 1000 m depth, and virtually no change below 2000 m. This water has evidently not yet been influenced by recently ventilated North Atlantic Deep Water (absolute CFC-11 < 0.1 pmol kg^{-1} in 2004). The midlatitude stations between these two extremes exhibit large station-to-station variability. In order to better visualize the vertical profiles and to facilitate comparison with the model, the modeled and measured profiles of ΔDIC and ΔpCFC from three selected regions are shown in Figure 11. The observations in the northern and southern zones are represented by only one station each so these profiles show more scatter, whereas zone #2 is an average. The averaged modeled profiles for the three boxes indicated in the map (Figure 3) are displayed in the bottom plots in Figure 11. Note that the magnitude of the modeled and observed ΔpCFC-11 and ΔDIC are comparable for all three zones, with the exception of the surface layers where the observations are affected by

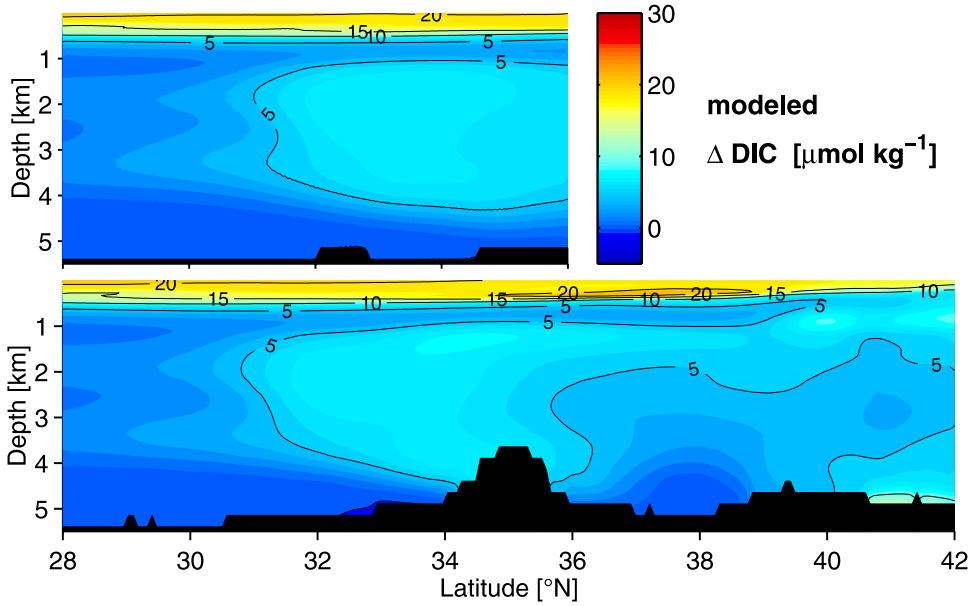

Figure 10. Sections of the annual average of modeled ΔC_{ant} between 1978 and 2001 for the two sections indicated in Figure 3.

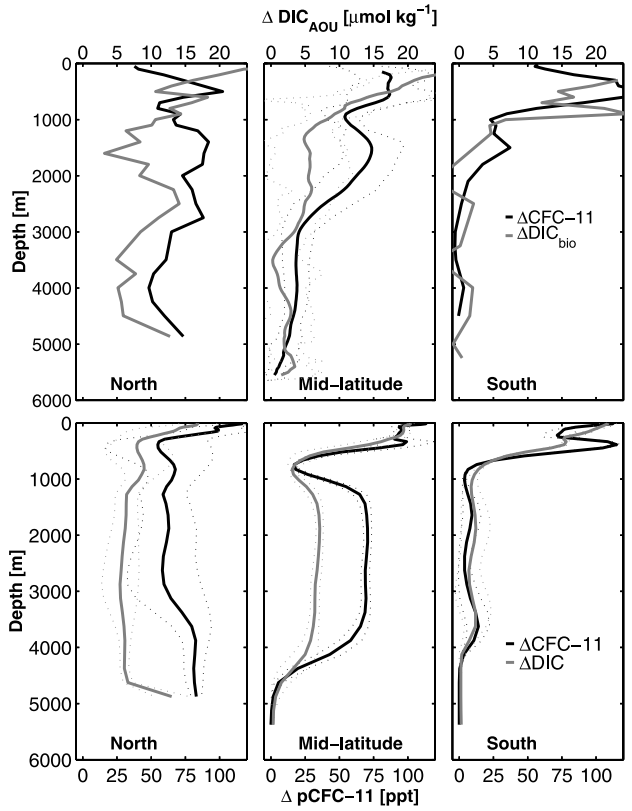

Figure 11. Relationship between ΔDIC and ΔpCFC-11. The gray line is the ΔDIC (μmol kg^{-1}), upper scale, and the black line is the ΔpCFC-11 (ppt), lower scale. (top) Observations, with the northern zone represented by station 181, the southern by station 173, and (top middle) an average of the other stations. (bottom) Modeled averaged ΔDIC and ΔpCFC for the three boxes indicated in Figure 3, roughly corresponding to the three zones of the observations. The thin, dotted lines are 1 standard deviation of the scatter in data between stations. In the observations, the upper ~500 m of the water column is dominated by seasonal effects.

seasonally variable conditions. The present study thus supports the model's ability to represent the ΔpCFC and ΔDIC distributions in the northwest Atlantic generally well when the known deficits of the model are taken into account, and it seems a valid approach to use the model to learn more about the distributions of ΔDIC and ΔCFC.

[35] Large differences between the ΔDIC and ΔpCFC-11 are evident for the LSW layer, particularly for the midlatitude stations, where the large ΔpCFC-11 are accompanied by only a modest ΔDIC. A measured CFC signal in a water mass, or an increase in CFC concentrations between two repeat surveys, would normally be assumed to have a corresponding increase of DIC resulting from the anthropogenic increase of atmospheric CO_2 [cf. *Körtzinger et al.*, 1999]. In fact, this is a fundamental assumption of several models and back-calculation techniques that are used to calculate the oceanic concentration of anthropogenic CO_2. On the basis of the observations presented here, it is clear that since TTO-NAS an intrusion of recently ventilated water (LSW) has carried large amounts of CFC, but possibly smaller amounts of anthropogenic DIC (relative to the respective atmospheric increases) into the study area. This can mostly, and best, be explained by the differences in the input functions. On timescales of ocean circulation (a few hundred years), the increase of C_{ant} is gradual in comparison to the rapid, almost pulse like, increase for the CFCs stating in the 1960's. This is illustrated in Figure 1, where the expected pCFC and C_{ant} concentrations for a typical Labrador Sea surface water is plotted versus time.

[36] Another illustrative way of viewing the difference in the time-dependent input function of the two components is shown in Figure 12. The modeled C_{ant} and pCFC-11 profiles of the three regions identified in Figure 3 are plotted relative to their contemporaneous surface value; that is, the surface is set to 100. The profiles thus represent the depth-dependent concentrations of the tracers normalized to their surface concentrations. Profiles are plotted for 5 different years (1960, 1970, 1980, 1990 and 2000). These plots can be compared with the bottom panels of Figure 11, where the difference between two such curves (not normalized) is shown. The C_{ant} profiles in Figure 12, top, show that the long-term gradual temporal increase of surface water C_{ant} tends to produce almost identical relative profiles. That is, the entire water column is tracking the relatively steady atmospheric increase. The situation for CFC-11 is however different. The lateral advection of the pulse-like increase of CFCs in the atmosphere starting in the 1960's as well as the recent reversal of the atmospheric trend, (Figure 1) is manifested as a sudden and dramatic increase of the relative pCFC-11 profiles at depth. This increase is particularly dramatic in the LSW layer for the midlatitude region, as well as for most of the water column in the northern region. These modeled profiles indicate that a dramatic increase in pCFC-11 can be expected at depth as waters ventilated during an earlier period of rapid atmospheric pCFC-11 increase reach this region, whereas at the same time, only a moderate increase in C_{ant} is expected. This is in almost perfect agreement with the observed, averaged profiles of the ΔDIC_{bio} and ΔpCFC-11 in Figure 11.

5.2. Transient Steady State

[37] We explore the modeled profiles in Figure 12 further in relation to the concept of "transient steady state" as pointed out by *Keeling and Bolin* [1967], later discussed by *Gammon et al.* [1982] evaluating CFC profiles from the North Pacific, and further explored by *Holforth et al.* [1998] discussing C_{ant} estimates in the South and North Atlantic. *Gammon et al.* [1982] showed that the vertical profiles of a conservative tracer with exponentially increasing surface concentration reaches a "transient steady state" after a time significantly larger than the surface growth timescale (time constant ~60 years for C_{ant}) for a one-dimensional system (i.e., no lateral advection, only diffusion and vertical advection). The C_{ant} profiles (Figure 12, top) are increasing equally over time throughout the whole water column for all areas; that is, the normalized profiles are found "on top of each other." They therefore seem to represent a "transient steady state," even though the C_{ant} is

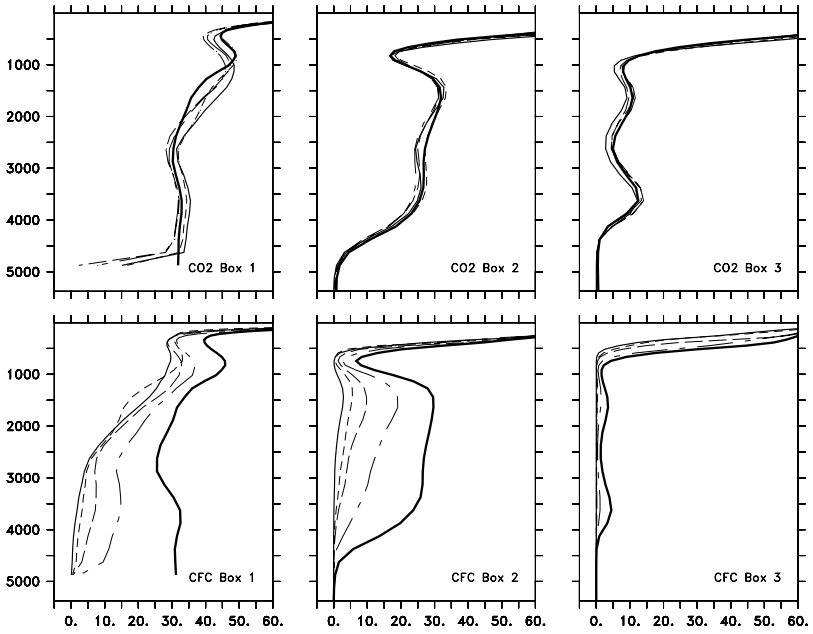

Figure 12. (top) Modeled C_{ant} and (bottom) pCFC-11 concentrations for the three boxes indicated on Figure 1. The profiles are normalized to surface concentrations and expressed in percent. The different years are represented by the following lines: 1960, thin solid line; 1970, short-dashed line; 1980, long-dashed line; 1990, dash-dotted line; and 2000, thick solid line.

supplied by lateral advection of recently ventilated waters. The advection is manifested in the shape of the depth profile, that is not exponentially decaying as it would for the no-advection, vertical-mixing case, but is rather composed of water masses with different advection times and mixing histories. The exception to this is found in the deep waters in the northern box that in year 2000 is affected by changes in lateral advection of the deep overflow water. The model results therefore demonstrate that the "transient steady state" concept is indeed valid for C_{ant} in this part of the North Atlantic Ocean. This has important implications for our ability to relate temporal increase of C_{ant} to the absolute inventory of C_{ant} in the North Atlantic, which we will explore elsewhere.

[38] It is clear from the pCFC-11 profiles that they are not in "transient steady state." The atmospheric CFC concentration has not been exponentially increasing for the last couple of decades, which violates the assumption made by *Gammon et al.* [1982].

5.3. Importance of Ocean Mixing for C_{ant} Calculations

[39] We further explore the property-property relation of both the observed and modeled ΔpCFC-11 and ΔDIC in more detail, Figure 13. The age calculations assume no mixing and should therefore be regarded as lower limits to the "real" age. Thus would a water parcel in contact with the atmosphere 20 years ago and not subsequently affected by mixing with older or younger water fall on the position of the red cross marked "20." The older water samples (CFC-12 age > 25 years), i.e., below the thermocline, follows the shape of the source function although with, on average, lower values of ΔDIC. As noted earlier, ΔpCFC-11 values higher than 120 ppt have been eroded away by mixing, so that there exists a mixing line between "young" (CFC age < 25 years) and "old" (CFC age > 25 years) samples.

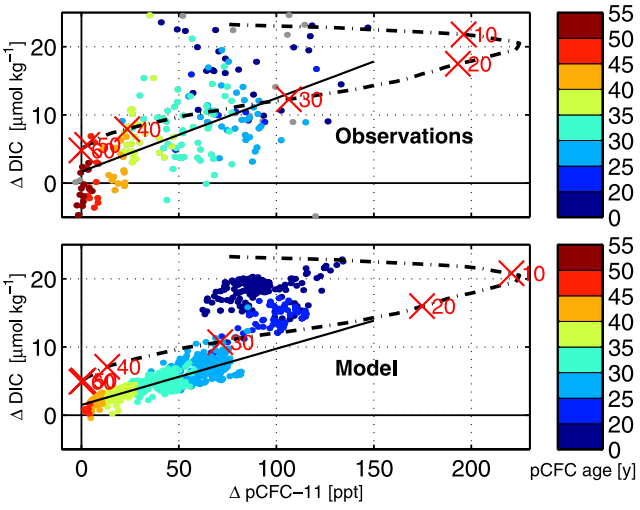

Figure 13. Figures of the relation of ΔpCFC-11 and ΔDIC versus depth. (top) Observed ΔDIC_{bio} and (bottom) model output. The shading of the data points denotes the CFC age (assuming no mixing); the thick dash-dotted line with "time markers" represents the historical relation between ΔDIC and ΔpCFC-11 calculated from the atmospheric source functions, with the same assumptions as in Figure 2. The solid black lines are linear fits of the data points with a CFC age > 25 years.

[40] It is well understood that C_{ant} estimates inferred from transient tracer data tends to be an overestimate if mixing effects are ignored [cf. *Hall et al.*, 2004; *Waugh et al.*, 2004; *Matsumoto and Gruber*, 2005]. This is also indicated by our observation of lower than expected ΔDIC relative to ΔpCFC-11 for the older samples (>25 years) in Figure 13. On the basis of the concept of transit time distributions (TTDs), the effect of mixing on the ΔDIC between 1980 and 1999 in the Newfoundland Basin has been calculated to be a reduction of the column uptake of about 25% compared to a scenario with no mixing [*Waugh et al.*, 2004, Figure 8C], which is mostly manifested in the deeper (older) part of the water column. That result is well in line with our result that shows, from both direct measurements and model calculations, the difference between a no-mixing scenario and the real ocean. The further effect of a temporal increase in the CO_2 air-sea disequilibrium due to rising atmospheric CO_2 [*Hall et al.*, 2004] cannot be determined from our data, but such a change would act in the same direction as the effect of mixing, i.e., to reduce the measured, or actual, ΔDIC_{bio} values.

5.4. C_{ant} in Low CFC Waters

[41] Several approaches to estimate C_{ant} inventories have made the assumption that water with zero, or low, CFC concentrations is essentially free of C_{ant} [e.g., *Gruber et al.*, 1996; *McNeil et al.*, 2003; *Sabine et al.*, 2004]. From Figure 13, it is clear that also for samples with pCFC age > 30 years in the North Atlantic, there has been a significant increase of C_{ant} over the last 23 years. The model results further reveals that for waters with a pCFC age of about 30 years, absolute concentrations of C_{ant} as high as 20 umol kg^{-1} can be found (results not shown). It is noticeable that the intercepts of both the theoretical, no-mixing, curve and our observation and modeled data points are positive; that is, even for samples with zero, or very small, ΔpCFCs there is still an anthropogenic increase in DIC detectable. The linear fit to data with an pCFC age > 25 years reveals an intercept of 1.7 ($r^2 = 0.58$) and 1.5 ($r^2 = 0.86$) μmol kg^{-1} for the direct comparison and the model, respectively. Our results therefore confirm that for parts of the ocean water with very low, or zero, CFC signal there can still be a significant contribution of anthropogenic CO_2 to overall inventories [e.g., *Wallace*, 2001; *Matsumoto and Gruber*, 2005]. Calculation of the magnitude of possible errors in C_{ant} inventories associated with assumption of no C_{ant} in CFC free waters is beyond the scope of this paper.

6. Conclusion

[42] Comparison of the increase of DIC and pCFC-11 concentration between 1981 and 2004 for 10 stations in the midlatitude North Atlantic Ocean reveals large differences in the patterns of increase of the two parameters. This is best explained by the differences in temporal input functions for C_{ant} and CFC-11, with the increase of atmospheric C_{ant} being gradual in comparison to the past rapid increase in CFC-11. We also observe that the ΔDIC is generally low compared to the theoretical ΔDIC, assuming no mixing, in relation to ΔpCFC-11. This is an expression of the importance of ocean mixing on the uptake of anthropogenic CO_2. We find that there is significant amounts of ΔDIC in waters with very low, or zero, ΔpCFC signal in the North Atlantic, implicating that zero CFC concentration do not equal zero C_{ant} signal. Our results suggest that estimates of anthropogenic CO_2 based on transient tracer data that fail to account for mixing tends to result in overestimations of the C_{ant} below the thermocline, whereas assuming there is no C_{ant} in water with zero, or low, CFC concentrations tends to underestimate C_{ant}. The model results suggest that the oceanic uptake of C_{ant} in the North Atlantic is in transient steady state; that is, the C_{ant} concentration increases proportionally over time through the whole water column in a manner that is directly related to the time-dependent surface concentration.

[43] **Acknowledgments.** The study was supported by the Deutsche Forschungsgemeinschaft (DFG) through SFB460 and grants for the M60/5 cruise program. Model integrations were performed at the Höchstleistungsrechenzentrum Stuttgart (HLRS) and Deutsches Klimarechenzentrum (DKRZ). We acknowledge the cooperation of the Captain, officers and crew of RV *Meteor*. The excellent measurements and good humor of the whole M60/5 team, especially the CO_2 and CFC-teams (Susann Grobe, Jens Schimanski, Jannes Ophey, Martina Schütt and Tim Fischer), are gratefully acknowledged. T. T. was supported by a Marie Curie Fellowship of the European Community program ''Improving Human Research Potential and the Socio-economic Knowledge Base'' under contract HPMF-CT-2002-01697. A. B. was supported by the BMBF project DEKLIM (contract 01 LD 0202). This study is funded also by grants from CARBOOCEAN.

References

Barnier, B., L. Siefridt, and P. Marchesiello (1995), Thermal forcing for a global ocean circulation model from a three-year climatology of ECMWF analyses, *J. Mar. Res.*, *6*, 363–380.

Böning, C. W., M. Rhein, J. Dengg, and C. Dorow (2003), Modeling CFC inventories and formation rates of Labrador Sea Water, *Geophys. Res. Lett.*, *30*(2), 1050, doi:10.1029/2002GL014855.

Boyer, T. P., and S. Levitus (1997), *Objective Analysis of Temperature and Salinity for the World Ocean on a 1/4° Grid*, *NOAA Atlas NESDIS 11*, Natl. Oceanic and Atmos. Admin., Silver Spring, Md.

Brewer, P. G., T. Takahashi, and R. T. Williams (1986), Transient tracers in the Ocean (TTO): Hydrographic data and carbon dioxide systems with revised carbon chemistry data, *CDIC Numer. Data Package NDP-004/R.*, 29 pp, Carbon Dioxide Inf. Anal. Cent., Oak Ridge, Tenn. (Available at http://cdiac.esd.ornl.gov/ftp/ndp004/ndp004.pdf)

Bullister, J. L., and R. F. Weiss (1988), Determination of CCl_3F and CCl_2F_2 in seawater and air, *Deep Sea Res., Part I*, *35*, 839–853.

Department of Energy (1994), Handbook of methods for the analysis of the various parameters of the carbon dioxide system in sea water, version 2, *Rep. ORNL/CDIAC-74*, Carbon Dioxide Inf. Anal. Cent., Oak Ridge, Tenn.

Dickson, A. G., and F. J. Millero (1987), A comparison of the equilibrium constants for the dissociation of carbonic acid in seawater media, *Deep Sea Res., Part A*, *34*, 1733–1743.

Doney, S. C., W. J. Jenkins, and J. L. Bullister (1997), A comparison of ocean tracer dating techniques on a meridional section in the eastern North Atlantic, *Deep Sea Res., Part 1*, *44*, 603–626.

Enting, I. G., T. M. L. Wigley, and M. Heimann (1994), Future emissions and concentrations of carbon dioxide: Key ocean/atmosphere/land analyses, *Tech. Rep. 31*, Div. of Atmos. Res., CSIRO, Melbourne, Victoria, Australia.

Friis, K. (2006), A review of marine anthropogenic CO_2 definitions: Introducing a thermodynamic approach based on observation, *Tellus, Ser. B*, *58*, 2–15.

Friis, K., A. Körtzinger, J. Pätsch, and D. W. R. Wallace (2005), On the temporal increase of anthropogenic CO_2 in the subpolar North Atlantic, *Deep Sea Res., Part I*, *52*, 681–698, doi:10.1016/j.dsr.2004.11.017.

Gammon, R. H., J. Cline, and D. Wisegarver (1982), Chlorofluoromethanes in the northeast Pacific Ocean: Measured vertical distributions and application as transient tracers of upper ocean mixing, *J. Geophys. Res.*, *87*(C12), 9441–9454.

Gent, P. G., and J. C. McWilliams (1990), Isopycnal mixing in ocean circulation models, *J. Phys. Oceanogr.*, *20*, 150–155.

Getzlaff, J., C. Böning, C. Eden, and A. Biastoch (2005), Signal propagation in the North Atlantic overturning, *Geophys. Res. Lett.*, *32*, L09602, doi:10.1029/2004GL021002.

Gruber, N. (1998), Anthropogenic CO_2 in the Atlantic Ocean, *Global Biogeochem. Cycles*, *12*(1), 165–191.

Gruber, N., J. L. Sarmiento, and T. F. Stocker (1996), An improved method for detecting anthropogenic CO_2 in the oceans, *Global Biogeochem. Cycles*, *10*(4), 809–837.

Hall, T. M., D. W. Waugh, T. M. W. Haine, P. E. Robbins, and S. Khatiwala (2004), Estimates of anthropogenic carbon in the Indian Ocean with the allowance for mixing and time-varying air-sea CO_2 disequilibrium, *Global Biogeochem. Cycles*, *18*, GB1031, doi:10.1029/2003GB002120.

Holforth, J., K. M. Johnson, B. Schneider, G. Siedler, and D. W. R. Wallace (1998), Meridional transport of dissolved inorganic carbon in the South Atlantic Ocean, *Global Biogeochem. Cycles*, *12*(3), 479–499.

Johnson, K., K. D. Willis, D. B. Butler, W. K. Johnson, and C. S. Wong (1993), Coulometric carbon dioxide analysis for marine studies: Maximizing the performance of an automated gas extraction system and coulometric detector, *Mar. Chem.*, *44*(2–4), 167–188.

Keeling, C. D., and B. Bolin (1967), The simultaneous use of chemical tracers in oceanic studies, *Tellus*, *19*, 566–581.

Kieke, D., M. Rhein, M. W. Smethie, D. A. Label, and W. Zenk (2006), Changes in the CFC inventories and formation rates of Upper Labrador Sea Water, 1997–2001, *J. Phys. Oceanogr.*, *36*, 64–86.

Kistler, R., et al. (2001), The NCEP/NCAR 50-year reanalysis, *Bull. Am. Meteorol. Soc.*, *82*, 247–268.

Körtzinger, A., M. Rhein, and L. Mintrop (1999), Anthropogenic CO_2 and CFCs in the North Atlantic Ocean: A comparison of man-made tracers, *Geophys. Res. Lett.*, *26*(14), 2065–2068.

Körtzinger, A., J. I. Hedges, and P. D. Quay (2001), Redfield ratios revisited: Removing the biasing effect of anthropogenic CO_2, *Limnol. Oceanogr.*, *46*(4), 964–970.

Lee, K., F. J. Millero, and R. Wanninkhof (1997), The carbon dioxide system in the Atlantic Ocean, *J. Geophys. Res.*, *102*(C7), 15,693–15,707.

Lee, K., et al. (2003), An updated anthropogenic CO_2 inventory in the Atlantic Ocean, *Global Biogeochem. Cycles*, *17*(4), 1116, doi:10.1029/2003GB002067.

Lewis, E., and D. W. R. Wallace (1998), CO2SYS—Program developed for the CO_2 system calculations, *Rep. ORNL/CDIAC-105,* Carbon Dioxide Inf. Anal. Cent., Oak Ridge, Tenn.

Lo Monaco, C., C. Goyet, N. Metzl, A. Poisson, and F. Touratier (2005), Distribution and inventory of anthropogenic CO_2 in the Southern Ocean: Comparison of three data-based methods, *J. Geophys. Res.*, *110*, C09S02, doi:10.1029/2004JC002571.

Matear, R. J., and B. I. McNeil (2003), Decadal accumulation of anthropogenic CO_2 in the Southern Ocean: A comparison of CFC-age derived estimates to multiple-linear regression estimates, *Global Biogeochem. Cycles*, *17*(4), 1113, doi:10.1029/2003GB002089.

Matsumoto, K., and N. Gruber (2005), How accurate is the estimation of anthropogenic carbon in the ocean? An evaluation of the ΔC^* method, *Global Biogeochem. Cycles*, *19*, GB3014, doi:10.1029/2004GB002397.

McNeil, B. I., B. Tilbrook, and R. J. Matear (2001), Accumulation and uptake of anthropogenic CO_2 in the Southern Ocean, south of Australia between 1968 and 1996, *J. Geophys. Res.*, *106*(C12), 31,431–31,445.

McNeil, B. I., R. J. Matear, R. M. Key, J. L. Bullister, and J. L. Sarmiento (2003), Anthropogenic CO_2 uptake by the ocean based on the global chlorofluorocarbon data set, *Science*, *299*, 235–239.

Mehrbach, C., C. H. Culberson, J. E. Hawley, and R. M. Pytkowitcz (1973), Measurements of the apparent dissociation constants of carbonic acid in seawater at atmospheric pressure, *Limnol. Oceanogr.*, *18*(6), 897–907.

Mintrop, L., F. F. Perez, M. Gonzalez-Davila, J. M. Santana-Casiano, and A. Körtzinger (2000), Alkalinity determination by potentiometry: Intercalibration using three different methods, *Sci. Mar.*, *26*(1), 23–37.

Pacanowski, R. C. (1996), Mom 2 version 2, documentation, user's guide and reference manual, *Tech. Rep. 3.2*, 332 pp., Geophys. Fluid Dyn. Lab., NOAA, Princeton, N. J.

Peng, T.-H., R. Wanninkhof, J. L. Bullister, R. A. Feely, and T. Takahashi (1998), Quantification of decadal anthropogenic CO_2 uptake in the ocean based on dissolved inorganic carbon measurements, *Nature*, *396*, 560–563.

Rhein, M., J. Fischer, W. M. Smethie, D. Smythe-Wright, R. F. Weiss, C. Mertens, D. H. Min, U. Fleischmann, and A. Putzka (2002), Labrador Sea Water: Pathways, CFC inventory, and formation rates, *J. Phys. Oceanogr*, *32*, 648–665.

Sabine, C. L., R. M. Key, K. M. Johnson, F. J. Millero, A. Poisson, J. L. Sarmiento, D. W. R. Wallace, and C. D. Winn (1999), Anthropogenic CO_2 inventory of the Indian Ocean, *Global Biogeochem. Cycles*, *13*(1), 179–198.

Sabine, C. L., et al. (2004), The oceanic sink for anthropogenic CO_2, *Science*, *305*, 367–371.

Sarmiento, J. L., J. C. Orr, and U. Siegenthaler (1992), A perturbation simulation of CO_2 uptake in an ocean general circulation model, *J. Geophys. Res.*, *97*(C3), 3621–3645.

Schlosser, P., J. L. Bullister, R. Fine, W. J. Jenkins, R. Key, J. Lupton, W. Roether, and W. M. J. Smethie (2001), Transformation and age of water masses, in *Ocean Circulation and Climate*, edited by J. Church, G. Siedler, and J. Gould, pp. 431–451, Elsevier, New York.

Siegenthaler, U., and F. Joos (1992), Use of a simple model for studying oceanic tracer distributions and the global carbon cycle, *Tellus, Ser. B*, *44*, 186–207.

Tanhua, T., and D. W. R. Wallace (2005), Consistency of TTO-NAS inorganic carbon data with modern measurements, *Geophys. Res. Lett.*, *32*, L14618, doi:10.1029/2005GL023248.

Walker, S. J., R. F. Weiss, and P. K. Salameh (2000), Reconstructed histories of the annual mean atmospheric mole fractions for the halocarbons CFC-11, CFC-12,CFC-113 and carbon tetrachloride, *J. Geophys. Res.*, *105*(C6), 14,285–14,296.

Wallace, D. W. R. (1995), Monitoring global ocean carbon inventories, report, 54 pp., Tex. A&M Univ., College Stn.

Wallace, D. W. R. (2001), Storage and transport of excess CO_2 in the oceans: The JGOFS/WOCE global CO_2 survey (2001), in *Ocean Circulation and Climate*, edited by G. Seidler, J. Church, and J. Gould, pp. 489–521, Elsevier, New York.

Wanninkhof, R. (1992), Relationship between gas exchange and wind speed over the ocean, *J. Geophys. Res.*, *97*(C5), 7373–7381.

Warner, M. J., and R. F. Weiss (1985), Solubilities of chlorofluorocarbons 11 and 12 in water and sea water, *Deep Sea Res., Part I*, *32*, 1485–1497.

Waugh, D. W., T. M. Hall, and T. W. N. Haine (2004), Transport times and anthropogenic carbon in the subpolar North Atlantic Ocean, *Deep Sea Res., Part I*, *51*, 1475–1491, doi:10.1016/j.dsr.2004.06.011.

Weiss, R. F., J. L. Bullister, R. H. Gammon, and M. Warner (1985), Atmospheric chlorofluoromethanes in the deep equatorial Atlantic, *Nature*, *314*, 608–610.

A. Biastoch and C. Böning, Ozeanzirkulation und Klimadynamik, Leibniz-Institut für Meereswissenschaften an der Universität Kiel, Duesternbrooker Weg 20, D-24105 Kiel, Germany. (abiastoch@ifm-geomar.de; cboening@ifm-geomar.de)

A. Körtzinger, T. Tanhua, and D. W. R. Wallace, Marine Biogeochemie, Leibniz-Institut für Meereswissenschaften an der Universität Kiel, Duesternbrooker Weg 20, D-24105 Kiel, Germany. (akoertziner@ifm-geomar.de; ttanhua@ifm-geomar.de; dwallace@ifm-geomar.de)

H. Lüger, 9 Seymour Avenue, PL48RA Plymouth, UK. (hlueger@gmx.com)